Cyclobutadiene–C$_{60}$ Adducts: N-Type Materials for Organic Photovoltaic Cells with High V$_{OC}$

*Ggoch Ddeul Han, William R. Collins, Trisha L. Andrew, Vladimir Bulović, and Timothy M. Swager**

New tetraalkylcyclobutadiene–C$_{60}$ adducts are developed via Diels–Alder cycloaddition of C$_{60}$ with in situ generated cyclobutadienes. The cofacial π-orbital interactions between the fullerene orbitals and the cyclobutene are shown to decrease the electron affinity and thereby increase the lowest unoccupied molecular orbital (LUMO) energy level of C$_{60}$ significantly (ca. 100 and 300 meV for mono- and bisadducts, respectively). These variations in LUMO levels of fullerene can be used to generate higher open-circuit voltages (V$_{OC}$) in bulk heterojunction polymer solar cells. The tetramethylcyclobutadiene–C$_{60}$ monoadduct displays an open-circuit voltage (0.61 V) and a power conversion efficiency (2.49%) comparable to the widely used P3HT/PCBM (poly(3-hexylthiophene/([6,6]-phenyl-C61-butyric acid methyl ester) composite (0.58 V and 2.57%, respectively). The role of the cofacial π-orbital interactions between C$_{60}$ and the attached cyclobutene group was probed chemically by epoxidation of the cyclobutene moiety and theoretically through density functional theory calculations. The electrochemical, photophysical, and thermal properties of the newly synthesized fullerene derivatives support the proposed effect of functionalization on electron affinities and photovoltaic performance.

1. Introduction

Bulk heterojunction (BHJ) polymer solar cells (PSCs), composed of conjugated polymer donors and small or macromolecule acceptors, are leading compositions in the quest for practical organic photovoltaic cells.[1,2] The bicontinuous nature of the phases in BHJ creates a large surface to volume ratio for efficient exciton dissociation, and facile and low-cost fabrication methods are compatible with large scale production.[3,4] Despite extensive efforts to improve the properties of the constituent materials and morphologies of BHJ systems, competing with the power conversion efficiency (PCE) of silicon-based solar cells remains a challenge.[5] In pursuit of ideal BHJ electronic

structures, researchers have developed low band gap p-type polymers that strongly absorb high fractions of the solar spectrum and assemble into desirable film morphologies.[6,7] Efforts to improve n-type acceptor components have included BHJs with small molecules such as 9,9′-bifluorenylidenes, perylenediimides, and vinazenes.[8–10] Nevertheless, fullerenes are presently the most widely used and highest performing materials in part due to their high electron affinities and low reorganization energies for electron transfer.[11] Tailoring the electronic structure of fullerene is therefore of interest, and reactions with organometallic reagents, transition-metal complexation, and radicals have been investigated to create new fullerenes for BHJs.[12–14] The reactivity of fullerene resembles that of an electron-deficient polyolefin, and as such, a dominant functionalization strategy has been to use cycloaddition reactions.[15,16] Noteworthy examples include the synthesis of PCBM ([6,6]-phenyl-C$_{61}$-butyric acid methyl ester) via 1,3-dipolar cycloaddition and indene–C$_{60}$ adducts from Diels–Alder reactions.[17–19]

Less-than-optimal band offsets at the BHJs can lead to energy loss and low open-circuit voltages in solar cells. In order to increase power conversion efficiencies, there have been efforts to increase the highest occupied molecular orbital–lowest unoccupied molecular orbital (HOMO$_D$–LUMO$_A$; A: acceptor, D: donor) gap which is often considered to be proportional to the open-circuit voltage.[20] Many polymer donors with alternating electron-rich and electron-poor units have been designed for optimized absorption of the solar spectrum. Decreasing the HOMO energy of the donor polymers can be accomplished by simple modifications of the electron-rich repeating units, but this typically leads to an expanded band gap that reduces the solar absorption efficiency, thereby giving a smaller short-circuit current density (J_{SC}).[21–23] As a result, an alternative, and perhaps more predictive, method is to increase the LUMO energy level of the fullerenes to create increased V_{OC}s. Most C$_{60}$ functionalization methods, including cycloaddition reactions, break the full conjugation of the C$_{60}$ π-system and generally decrease the electron affinity and raise the LUMO level.[24] The extent of this change varies depending on the nature of the functional groups attached to the C$_{60}$ core. The decreased relative electron affinity of C$_{60}$ is measured by the change of the onset

G. D. Han, Dr. W. R. Collins, Prof. T. M. Swager
Department of Chemistry
Massachusetts Institute of Technology
Cambridge, MA 02139, USA
E-mail: tswager@mit.edu
Dr. T. L. Andrew, Prof. V. Bulović
Department of Electrical Engineering and Computer Science
Massachusetts Institute of Technology
Cambridge, MA 02139, USA

ADVANCED
FUNCTIONAL
MATERIALS
www.afm-journal.de

Materials
Views
www.MaterialsViews.com
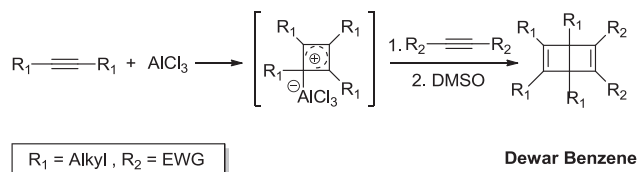
Scheme 1. AlCl$_3$-Assisted Diels–Alder Reaction of Alkynes

Figure 1. Structures of functionalized fullerenes.

reduction potential or the calculated LUMO level.[25,26] In this context, there has recently been interest in indene–C$_{60}$ acceptors because these materials exhibit ca. 50–170 meV reduced electron affinities (higher LUMO) relative to PCBM.[27] It would appear that the short distance between the C$_{60}$ π-system and the π-orbitals of the addend aromatic ring of the indene affects the LUMO energy.

To expand upon the hypothesis that cofacial π-orbital interactions between C$_{60}$ and an attached group can effectively raise the fullerene LUMO levels, we have targeted a new functionalization method that makes use of the well-known zwitterionic AlCl$_3$–cyclobutadiene adducts. The release of the cyclobutadienes by treatment of AlCl$_3$–cyclobutadiene adducts with weak Lewis bases has been found to result in Diels–Alder reactions with alkynes (**Scheme 1**)[28] to give Dewar benzene products that have fairly small angles (114.6–114.9°) between two cyclobutene rings.[29] As a result, we rationalized that Diels–Alder adducts of similarly generated cyclobutadiene adducts with fullerenes could give rise to strong cofacial π-orbital interactions.

In this study we report the syntheses of mono- and multiadducts of tetramethylcyclobutadienes (**Scheme 2**) and tetrabutyl-cyclobutadienes to fullerenes (**Figure 1**). The electrochemical, photophysical, and thermal properties of these new fullerenes have been studied, and their use in photovoltaic devices with poly(3-hexylthiophene) (P3HT) has been evaluated in comparison with PCBM. Tetramethylcyclobutadiene–C$_{60}$ mono-, bis-, and trisadducts (TMCB-Mono, TMCB-Bis, and TMCB-Tris) all exhibited higher open-circuit voltages than that of PCBM, and TMCB-Mono showed comparable power conversion efficiency (2.49%) to PCBM (2.57%) devices under the identical conditions. Lastly, the π-orbital interactions between cyclobutene and the C$_{60}$ cage were probed by removing the appended double bond by epoxidation. The increased electron affinity of the cyclobutane–epoxide–C$_{60}$ was measured by cyclic voltammetry and calculated using density functional theory. All of our results are consistent with the hypothesis that π–π orbital interactions are an effective means to adjust the fullerene LUMO levels.
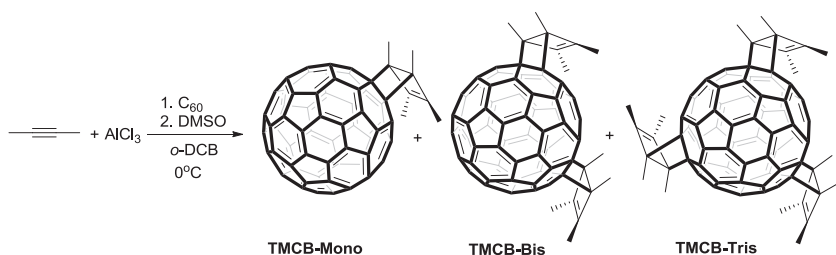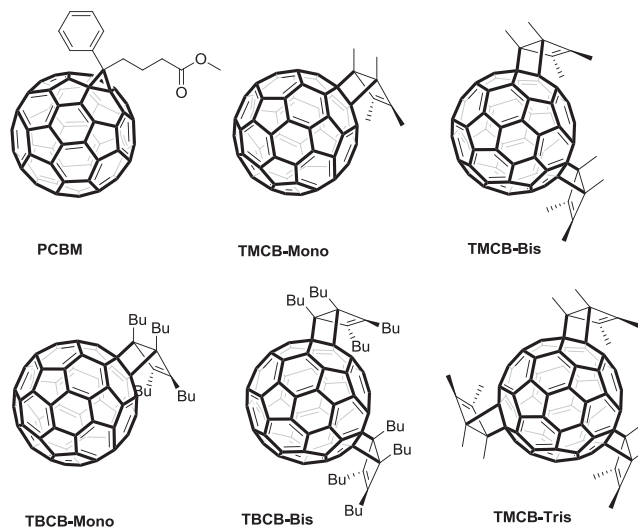
2. Results and Discussion

2.1. Syntheses of Tetraalkylcyclobutadiene–C$_{60}$ Adducts

It is well-known that aluminum chloride reacts with internal alkynes to generate cyclobutadiene intermediates with a σ-bonded aluminum moiety (Scheme 1).[28] The intermediate cyclobutadiene, which is liberated by addition of dimethyl-sulfoxide, is very reactive in [4 + 2] cycloaddition reactions either as a diene (Scheme 1) or as a reactive alkene.[30] C$_{60}$ is a potent dienophile[31] and new n-type C$_{60}$ derivatives are created via Diels–Alder reactions with the in situ generated tetraalkylcyclobutadienes.

The reactions were run under moisture-free conditions wherein the reaction of 2-butyne and aluminum chloride was first combined with C$_{60}$ and subsequent treatment with DMSO produced tetramethylcyclobutadiene–C$_{60}$ mono-, bis-, and trisadducts (Scheme 2). By varying the molar ratio of the alkyne, aluminum chloride, and C$_{60}$, we were able to selectively increase the yield of each product in the mixture. In many cases, the syntheses of functionalized fullerenes involve tens of equivalents of the non-fullerene reagents to ensure a high-yielding functionalization.[27,32] In contrast, four equivalents of 2-butyne relative to C$_{60}$ produce monoadduct and bisadduct in isolated respective yields of 32% and 17% after rigorous purification. Generation of four equivalents of cyclobutadiene (8 eq. of 2-butyne) increases the isolated yield of the pure trisadduct to 8%. It is also the case that the syntheses of fullerene derivatives by Diels–Alder reactions often require long reaction times,[33] and high temperatures such as refluxing o-dichlorobenzene (b.p. 180.5 °C).[32] The cyclobutadiene addition was carried out at low temperatures (between 0 °C and room temperature) with reaction times of less than 2 h. After the reaction, the mixture of fullerene adducts was separated by HPLC using a 5PBB Cosmosil column with toluene elution. ^{1}H and

Scheme 2. Synthesis of TMCB Fullerenes.

www.MaterialsViews.com

ADVANCED
FUNCTIONAL
MATERIALS
www.afm-journal.de

FULL PAPER

^{13}C nuclear magnetic resonance (NMR) spectroscopy as well as high-resolution mass spectrometry (HRMS) confirmed the attachment of the cyclobutene moiety. The similar procedure provided other tetraalkylcyclobutadiene–C_{60} adducts starting with symmetric internal alkynes such as 3-hexyne, 4-octyne, and 5-decyne (Supporting Information Scheme S1). The longer alkyl products provide for higher solubility in organic solvents such as chloroform, dichloromethane, and toluene. Longer chains disfavor trisadduct formation, presumably due to the steric strain on the C_{60} surface. For example, for the functionalization starting with 5-decyne, we could not observe the trisadduct even when using 16 equivalents of this alkyne. Figure 1 details the representative five new functionalized fullerenes selected for further investigation and the well-known PCBM.

2.2. Electrochemical Properties

C_{60} has triply-degenerated low-lying LUMO energy levels and thereby can be reduced by up to six electrons.[34] A series of cyclic voltammograms in **Figure 2** shows that three or four reversible redox waves are retained in the functionalized fullerenes under anhydrous air-free conditions, relative to the ferrocene/ferrocenium (Fc/Fc$^+$) internal standard peaks at ca. 200 mV ($\pm$0.5 mV).

The monoadducts (TMCB-Mono and TBCB-Mono) exhibited four reversible redox peaks (Figure 2a,b), which are all shifted to negative potentials by ca. 100 mV as compared to PCBM, and the bisadducts showed an additional ca. 200 mV shift relative to the monoadducts. The measured half-wave potentials are listed in **Table 1** together with the estimated LUMO energy levels relative to the vacuum level. The cyclic voltammogram of the trisadduct contained three major sets of the redox peaks, as well as another set of peaks, which we assume to be a persistent tetrakisadduct impurity (Figure 2a). Despite the less defined features, it is clear that the three main redox waves are further shifted by about 200 mV as compared to the bisadduct. The reversible sets of redox curves shown in Figure 2a,b confirm that the functionalization preserves the key electronic accepting characteristics of C_{60}. The pronounced negative shifts of redox curves and the corresponding increase of LUMO energy levels relative to PCBM (90 meV for TMCB-Mono, 260 meV for TMCB-Bis, and 450 meV for TMCB-Tris) are considerably greater than the indene–C_{60} mono- and bisadducts (50 meV and 170 meV, respectively).[27] This behavior is consistent with our designs that make use of the small

(a)

(b)
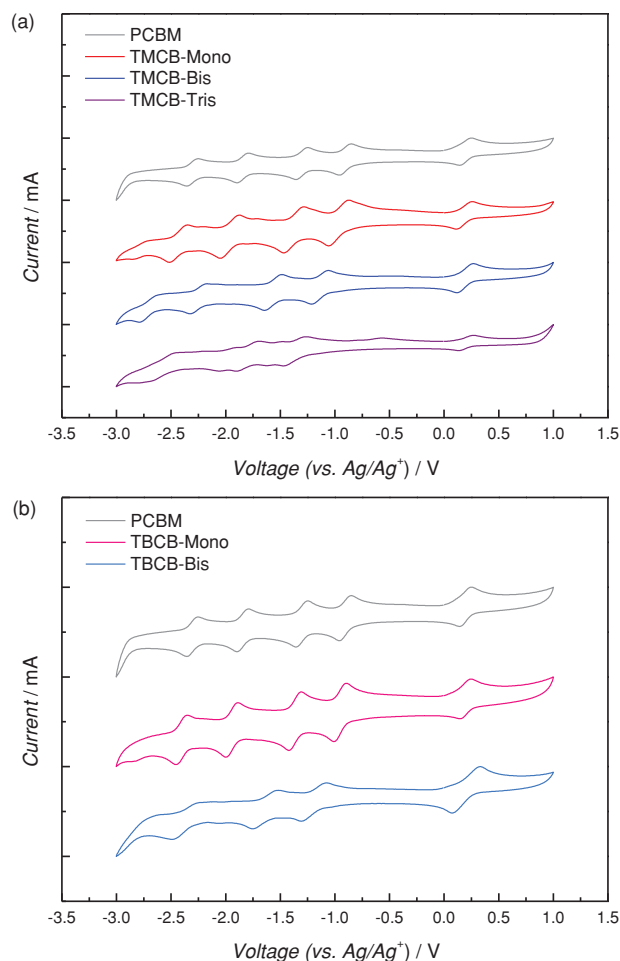
Figure 2. Cyclic voltammograms of a) PCBM and TMCB mono-, bis-, and trisadducts and b) TBCB mono-, and bisadducts (under N$_2$, 0.1 M Bu$_4$NPF$_6$ in toluene/acetonitrile (4:1), Pt (WE), Pt wire (CE), Ag/AgNO$_3$ (RE), scan rate 0.1 V/s, Fc/Fc$^+$ internal standard $E_{1/2}$ at 0.20 V).

angles between fused four-membered rings, which increases the π-orbital interaction between the pendant cyclobutene moiety and C_{60} centered states. It is not straightforward to explain the difference in LUMO shifts of indene–C_{60} and cyclobutadiene–C_{60}. The proximity of the addend π-orbitals to C_{60} surface, or the

Table 1. HOMO and LUMO energy levels calculated from UV–vis absorption and cyclic voltammetry.

C_{60} derivative	E_1 [V][a]	E_2 [V]	E_3 [V]	E_{onset} [V][b]	LUMO [eV][c]	λ_{onset} [nm][d]	HOMO [eV][e]	E_{gap} [eV][f]
PCBM	−0.90	−1.31	−1.85	−0.77	−3.83	723	−5.55	1.72
TMCB-Mono	−0.96	−1.38	−1.97	−0.86	−3.74	738	−5.42	1.68
TMCB-Bis	−1.14	−1.57	−2.25	−1.03	−3.57	746	−5.24	1.67
TMCB-Tris	−1.37	−1.79	−2.57	−1.22	−3.38	697	−5.16	1.78
TBCB-Mono	−0.96	−1.36	−1.94	−0.88	−3.72	740	−5.40	1.68
TBCB-Bis	−1.19	−1.64	−2.38	−1.10	−3.50	751	−5.15	1.65

[a] Half-wave potential, 0.5 (E_{pa}+ E_{pc}); E_{pa}, anodic peak potential; E_{pc} cathodic peak potential; [b] Onset reduction potential; [c] LUMO (eV) = −e (E_{onset} + 4.60); [d] Onset absorption wavelength; [e] HOMO = LUMO−E_{gap} [eV]; [f] Band gap = hc/λ_{onset}, converted [J] to [eV]; h, Planks constant; c, speed of light.

**ADVANCED
FUNCTIONAL
MATERIALS**
www.afm-journal.de

*Materials
Views*
www.MaterialsViews.com

angle between two rings, of either compound has not been determined and crystal structures have not been obtained to date. The different extent of LUMO shifts could be also influenced by other factors, given two dissimilar addend structures.

The cyclic voltammograms of TMCB-adducts and TBCB-adducts are similar in terms of the shape and the positions of potentials, but the TBCB-adducts exhibit slightly more negative redox potentials. Considering the higher LUMOs of the TBCB-series we expect a slightly higher V_{OC} in photovoltaic devices relative to those obtained for TMCB-adducts.

2.3. Photophysical Properties

The visible and near-infrared spectral absorptions of BHJ devices are a major determinant of solar cell efficiencies. J_{SC} is dependent on the number of charge carriers generated and their mobility.[20] Considerable efforts have focused on creating donor polymers with band gaps that match the solar spectrum. Although J_{SC} is generally dominated by the photon collection of the donor polymer, stronger visible light absorption of the acceptors can also contribute to light harvesting. Specifically, the weak optical absorptions of PCBM are considered a limitation and have led to interest in more costly C_{70} acceptor materials.[35] In **Figure 3**, we show comparative absorption spectra (400–800 nm) of our new fullerene derivatives relative to PCBM. The cyclobutadiene functionalized fullerenes exhibited the similar or higher absorptivity relative to PCBM. A more intense absorption was observed for the higher adducts, which is consistent with desymmetrization of fullerenes. The weak spikes around 430 nm for TMCB- and TBCB-Mono are characteristic for 1,2-addition products, which confirms the structures depicted in Scheme 2. A hypothetical 1,4-adduct, which would form if C_{60} acted as a diene and cyclobutadiene as a dienophile, would exhibit a broad absorption band around 450 nm, instead.[36–39] The absorption peaks around 430 nm are slightly red-shifted from that of PCBM. Additionally, the bis- and trisadducts showed broader absorptions as a result of the fact that they are a mixture of regioisomers. Based upon their absorption properties these new fullerene derivatives appear to offer advantages over PCBM in terms of the higher absorptivity and the red-shifted absorption edge around 700 nm. The absorption edge wavelengths, λ_{onset}, vary from 697 to 751 nm, and longer wavelengths were observed for bisadducts than monoadducts and PCBM (Table 1). The trisadduct is a 56-π-electron fullerene and deviates from the trend with a small value of λ_{onset}. The band gaps and the HOMO energy levels of the fullerenes were calculated from λ_{onset} and the first reduction wave, and are summarized in **Figure 4** and Table 1.

2.4. Thermal Properties

The thermal stability of the molecules was determined by thermogravimetric analysis (TGA), which revealed weight loss of less than 5% at 200 °C under N_2 atmosphere (Supporting Information Figure S2). All functionalized fullerenes are less stable than pristine C_{60} which has outstanding thermal stability up to 500–600 °C.[40] C_{60} derivatives often display a change in morphology or decomposition at around 150 °C, and the typical annealing
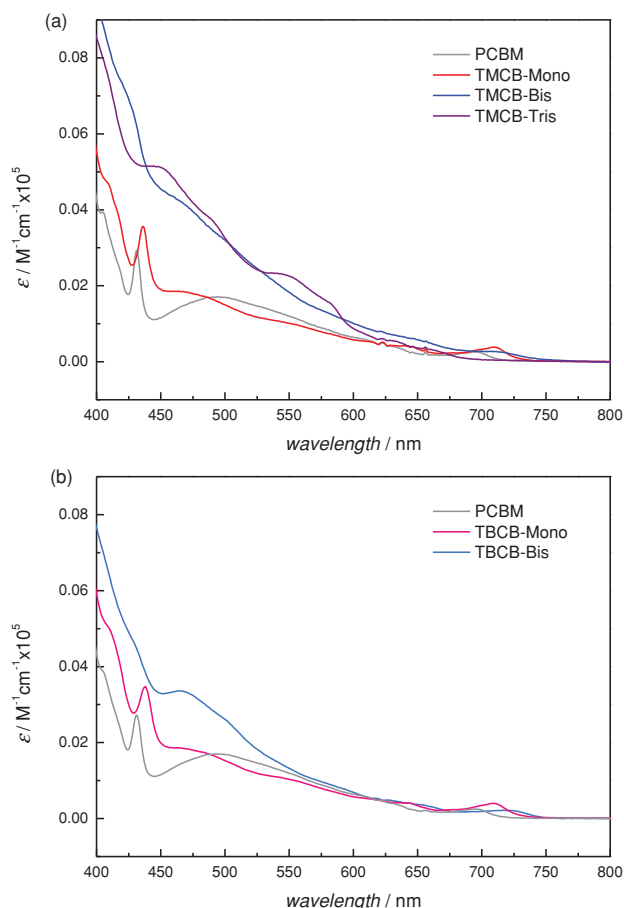
Figure 3. UV–vis absorption spectra of a) PCBM (2.4×10^{-5} M), TMCB-Mono (2.5×10^{-5} M), Bis (2.4×10^{-5} M), and Tris (2.0×10^{-5} M), and b) TBCB-Mono (2.3×10^{-5} M), and Bis (1.3×10^{-5} M) in CHCl₃.

temperatures used in polymer solar cell fabrications affect their performance. To further investigate the thermal properties of the fullerene adducts and the effects of annealing, we conducted differential scanning calorimetry (DSC) experiments over the
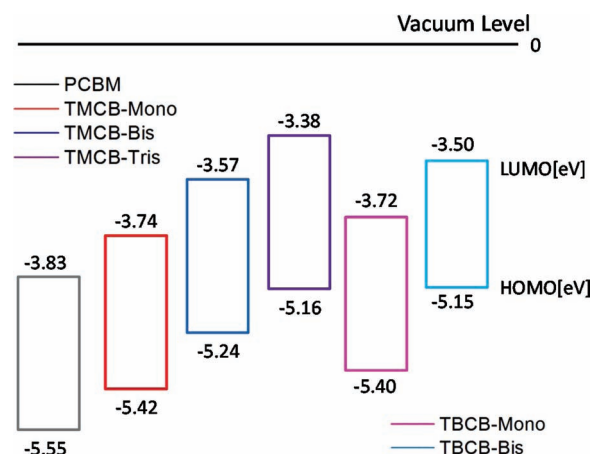
Figure 4. HOMO–LUMO energy diagram of fullerene derivatives. The energy levels were drawn relative to the vacuum level that is by definition set to zero.

www.MaterialsViews.com

ADVANCED
FUNCTIONAL
MATERIALS
www.afm-journal.de

FULL PAPER

range from 25 to 200 °C (Supporting Information Figure S3). In the first cycle, a strong and broad exothermic heat flow was observed for TMCB-Bis and Tris from 90 to 150 °C and 80 to 190 °C, respectively (Supporting Information Figure S3a).

In contrast, the TMCB-Mono displays a small endothermic peak which starts to appear at ca. 110 °C, which is likely due to loss of residual toluene (b.p. 111 °C). The second DSC cycles were featureless for all of the compounds (Supporting Information Figure S3b). The mono- and bisadducts of tetrabutylcyclobutadiene exhibited relatively featureless heat flow to their tetramethyl counterparts (Supporting Information Figure S3c,d).

BHJs formed with P3HT after annealing at 150 °C for 20 min were studied by atomic force microscopy (AFM) (**Figure 5**).
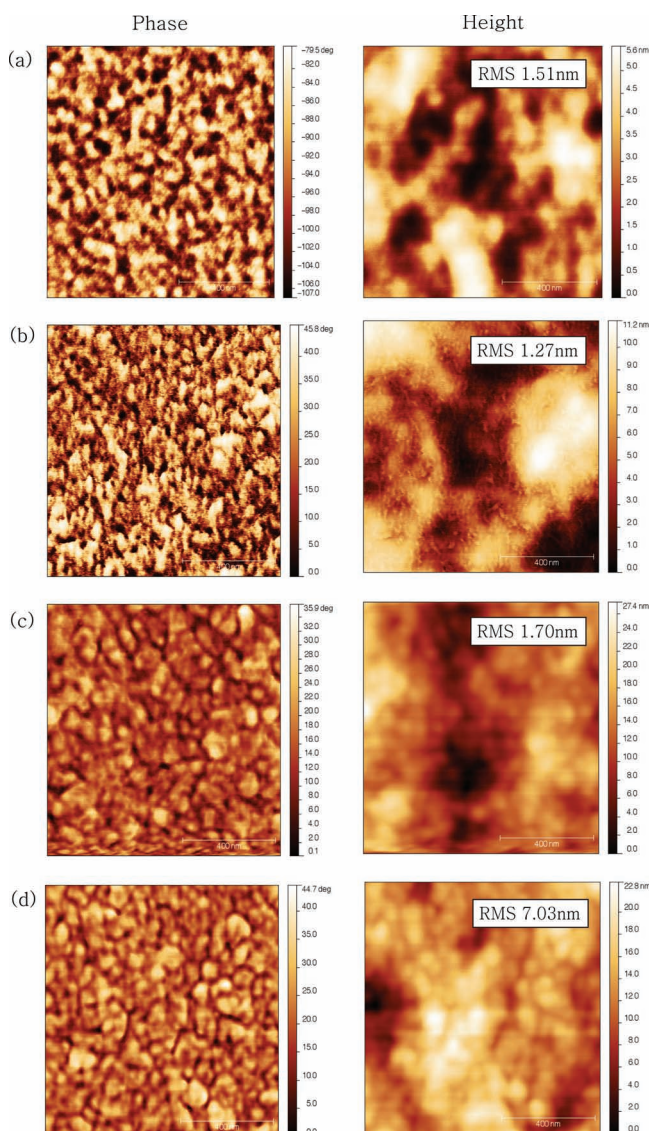
Figure 5. Tapping-mode atomic force microscopy (1 μm window) phase and topography images of the films prepared from a) PCBM, b) TMCB-Mono, c) TMCB-Bis, and d) TMCB-Tris. P3HT was used as a donor for all devices. PEDOT:PSS was used as the underlayer. All BHJs were annealed at 150 °C for 20 min. Root-mean-square roughness was measured and indicated in the topography images.

The larger grain sizes (root-mean-square roughness) and more pronounced phase separation were observed in the films with higher adducts. The P3HT/TMCB-Mono morphology most closely resembled the roughness of the P3HT/PCBM blend. We were interested in determining if any of the features observed for the higher adducts in the DSC and AFM reflected thermal decomposition or only morphology changes. Indeed our new fullerene derivatives could be susceptible to retro-cycloaddition reactions as other fullerene cycloadducts.[41,42] In order to investigate this, we measured the ^{1}H NMR spectra of the fullerene derivatives after three DSC cycles (25–200 °C, 10 °C/min) (Supporting Information Figure S4a,b). The TMCB-Bis gained the peaks assignable to TMCB-Mono, and TMCB-Tris gained the peaks indicating the generation of TMCB-Mono and TMCB-Bis. As a result, it is possible that larger phase separation of the BHJ layers with the multiadducts is related to conversion of the fullerene multiadducts into less-functionalized adducts upon annealing. The ^{1}H NMR spectra of the TMCB-Mono, TBCB-Mono, and TBCB-Bis after being subjected to three DSC cycles did not display any detectable changes thereby reconfirming their superior thermal stability as compared to the TMCB multiadducts. To determine if crystallization might also be responsible for the exothermic DSC transitions of the TMCB multiadducts at high temperatures, we conducted X-ray diffraction experiments (Supporting Information Figure S5a,b). TMCB and TBCB monoadducts are a single regioisomer, presumably fused to C_{60} in [6,6]-closed fashion as usual Diels–Alder cycloaddition products of C_{60},[43–45] and exhibit microcrystallinity. The butyl groups on cyclobutadiene–C_{60}, as expected, produce a larger lattice spacing (11.2 Å) than methyl groups (10.1 Å). For multiadducts, the mixture of isomers reduced the crystallinity of the sample, and TMCB-Bis remained in an amorphous state even after three DSC cycles. As a result, the observed DSC exothermic transitions for the multiadducts are most likely the result of retro-cycloaddition reactions. In an attempt to produce a more stable analog, the reaction of C_{60} and naphthocyclobutadiene was conducted. However, the reaction did not proceed, presumably as a result of the fact that the tetraalkylcyclobutadiene behaves as the diene in the Diels–Alder reaction and naphthocyclobutadiene would only be expected to behave as the dienophile.

2.5. Organic Photovoltaic Performances

Figure 6 details current density versus voltage (J–V) characteristics under illumination of select P3HT/fullerene BHJ solar cells. Specifically TMCB-Mono, Bis, and Tris are compared to the well-known P3HT/PCBM system. As predicted based on the LUMO energy levels, TMCB-Mono gives a higher open-circuit voltage than PCBM. The P3HT/TMCB-Mono system also displays a short-circuit current density, fill factor, and PCE (η) comparable to the P3HT/PCBM device. The J–V curve of TMCB-Bis displays a higher V_{OC}, consistent with its higher LUMO level, but a much lower J_{SC} and decreased fill factor lead to poor efficiency. We expect that the thermal instabilities of the higher fullerene cyclobutadiene adducts contributes to lower efficiencies. The performance of the P3HT/TMCB-Tris cell displays even lower J_{SC}. Field-effect mobilities of electrons are

**ADVANCED
FUNCTIONAL
MATERIALS**

www.afm-journal.de

FULL PAPER

*Materials
Views*
www.MaterialsViews.com
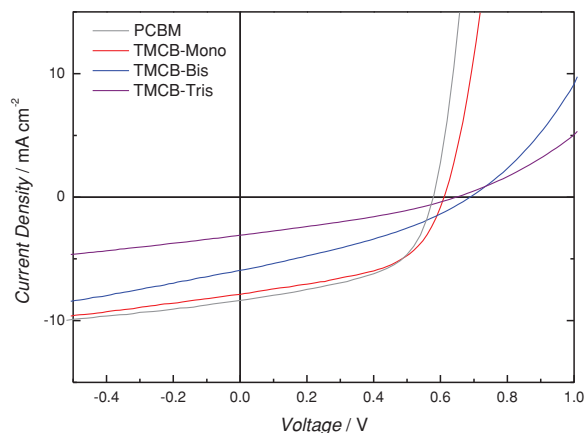
Figure 6. Current density–voltage (*J–V*) characteristics of bulk hetero-junction PSCs under AM 1.5 illumination at 100 mW/cm². ITO (150 nm)/PEDOT:PSS (40 nm)/P3HT:fullerenes (75 nm)/Ca (25 nm)/Al (80 nm) used for device fabrication.

also decreased for the higher adducts in comparison to TMCB-Mono and the standard PCBM. 2.53×10^{-3} cm²/V·s for PCBM, 1.08×10^{-3} cm²/V·s for TMCB-Mono, 1.07×10^{-5} cm²/V·s for TMCB-Bis, and 1.34×10^{-6} cm²/V·s for TMCB-Tris were obtained. An interesting feature is that the open-circuit voltage of TMCB-Tris is smaller than that of TMCB-Bis. This discrepancy might result from the excessive decomposition of Tris upon annealing. In general, the open-circuit voltages of the BHJ polymer-fullerene films are influenced by intermolecular interactions in the solid state. Thus, they can exhibit quantitatively non-linear correlation with HOMO$_D$–LUMO$_A$ gaps, predicted by the solution-state measurements. Additionally, we note that the V_{OC} in organic BHJ solar cells is recombination limited.[46] Since we observe non-ideal BHJ morphologies with some of our fullerene adducts, which increases the rate of bimolecular recombination across the donor-acceptor interface, we hypothesize that part of the observed discrepancy in V_{OC} trends is also due to increased recombination. Correspondingly, the PCE (**Table 2**) of P3HT/TMCB-Mono (2.49%), comparable with that of P3HT/PCBM (2.57%), and the smaller values for P3HT/TMCB-Bis (1.35%) and P3HT/TMCB-Tris (0.65%) were consistent with the degree of phase separation and root-mean-square roughness discovered on AFM images.

To obtain the optimized performance of fullerene adducts with longer alkyl chains, we annealed the devices with TBCB-Mono and TBCB-Bis at 90 °C (Supporting Information Figure S6). P3HT/TBCB-Mono blend produced higher V_{OC} (0.64 V) and J_{SC}

Table 2. Characteristics of OPV Devices[a]

	TMCB-Mono	Bis	Tris	PCBM
J_{SC} [mA/cm²]	7.86	5.92	3.13	8.35
V_{OC} [V]	0.61	0.69	0.65	0.58
FF [%]	0.52	0.33	0.32	0.53
η [%]	2.49	1.35	0.65	2.57

[a]Definitions: short-circuit current density, J_{SC}; open-circuit voltage, V_{OC}; fill factor, FF; PCE, η.
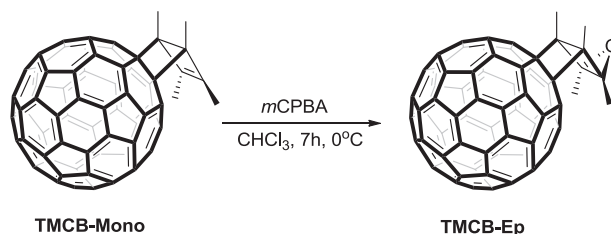
Scheme 3. Epoxidation of TMCB-Mono.

(9.72 mA/cm²) compared to P3HT/PCBM (Supporting Information Figure S6), but the increased resistance in the blend resulted in lower fill factor and comparable PCE (2.43%). The decreased V_{OC} (0.61 V) and J_{SC} (1.37 mA/cm²) of P3HT/TBCB-Bis cell led to poor PCE (0.23%), thus reconfirming that less desirable performances are obtained from our multiadducts. In addition, the comparison of the *J–V* curves from different annealing conditions (90 and 120 °C) reflected the destructive effect of thermal annealing at high temperatures on the cells.

2.6. Elimination of π-Orbital Interaction

To chemically probe our hypothesis that large decrease in electron affinity in the cyclobutadiene-fullerenes is the result of strong interactions between the cyclobutene double bond and the C$_{60}$ π-system, we devised a simple experiment to remove the double bond. Several reactions were attempted, but the most straightforward and the highest-yielding reaction was epoxidation with 3-chloroperbenzoic acid (*m*CPBA) (**Scheme 3**). The reaction proceeded with 96% yield, and the product (TMCB-EP) had significantly different polarity from the starting material, which facilitated purification. The identity of the product was supported by ^{1}H and ^{13}C NMR spectra as well as HRMS. Epoxidation of TBCB-Mono was unsuccessful presumably as a result of steric hindrance around the reaction site, and only starting material was recovered.

Cyclic voltammetry of TMCB-Ep (**Figure 7**) exhibited four reversible redox peaks like other monoadducts, but half-wave
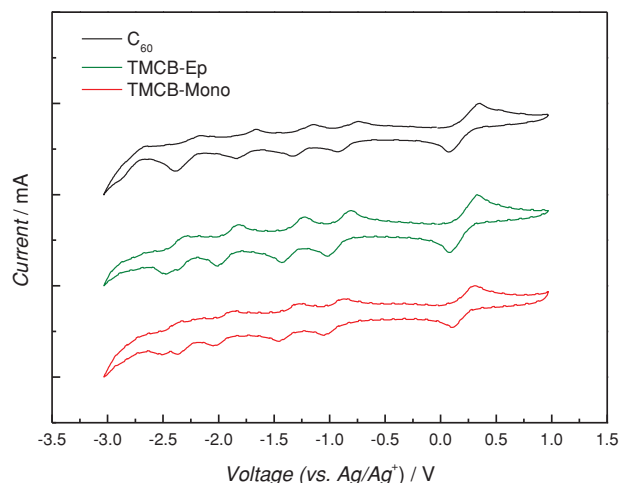
Figure 7. Cyclic voltammograms of C$_{60}$, TMCB-Ep, and TMCB-Mono (under N$_2$, 0.1 M Bu$_4$NPF$_6$ in toluene/acetonitrile (4:1), Pt (WE), Pt wire (CE), Ag/AgNO$_3$ (RE), scan rate 0.1 V/s, Fc/Fc$^+$ internal standard $E_{1/2}$ at 0.20 V).

Table 3. Electrochemical characteristics and LUMO energy levels of C_{60}, TMCB-Ep, and TMCB-Mono.

	E_1 [V][a)]	E_2 [V]	E_3 [V]	E_{onset} [V][b)]	LUMO [eV][c)]
C_{60}	−0.84	−1.24	−1.75	−0.75	−3.85
TMCB-Ep	−0.91	−1.34	−1.92	−0.81	−3.79
TMCB-Mono	−0.97	−1.38	−1.95	−0.86	−3.74

[a)]Half-wave potential (V), 0.5 ($E_{pa} + E_{pc}$); E_{pa}, anodic peak potential; E_{pc} cathodic peak potential; [b)]Onset reduction potential; [c)]LUMO (eV) = $-e$ (E_{onset} + 4.60).

potentials were located approximately half way between those of pristine C_{60} and the TMCB-Mono compound. In **Table 3**, the half-wave potentials of TMCB-Ep were summarized. The difference between LUMO energy levels of C_{60} and TMCB-Ep is 60 meV, and the gap between those of TMCB-Ep and TMCB-Mono is 50 meV. From this observation, we conclude that orbital interactions between the cofacial cyclobutene and C_{60} π-systems contribute to the observed LUMO raising. The electron affinity of TMCB-Ep was still lower than that of C_{60} and this is presumably the result of the σ-π hyperconjugative interactions.

To further support this assertion, we conducted quantum-chemical density functional theory (DFT) calculations (B3LYP functional/6-31G (d,p) basis set) of TMCB-Mono and TMCB-Ep. The geometry optimized structures (Supporting Information Figure S7a,b) had HOMO and LUMO energy levels of −5.58 and −3.04 eV for TMCB-Mono, and −5.69 and −3.16 eV for TMCB-Ep (Supporting Information Figure S8a,b). These results also indicated that epoxidation of the cyclobutene moiety decreased the LUMO level. The calculated distances between C_{60} cage and the attached functional groups were 3.05 and 3.10 Å for TMCB-Mono and TMCB-Ep, sufficiently short to allow for cofacial π-orbital interactions.[47] It is apparent in the LUMO representations (side and front views on Supporting Information Figure S8a) of TMCB-Mono that the wavefunction on the double bond of the cyclobutene moiety and that on the adjacent C_{60} π-orbital possess the opposite signs. It is believed that the LUMO level of C_{60} is raised effectively due to this close π–π interaction between the two moieties. On the other hand, for TMCB-Ep (Supporting Information Figure S8b), the hyperconjugative interaction between the C–H σ-bonds of methyl groups and C_{60} π-system is outstanding for most of the MOs rather than cofacial π interaction. Therefore, we could theoretically support the concept of the structural design of cyclobutadiene–C_{60} for efficient cofacial π interaction and the experimental results.

3. Conclusions

Two families of tetraalkylcyclobutadiene–C_{60} adducts were generated via Diels–Alder cycloaddition reactions between in situ generated cyclobutadiene intermediates and C_{60}. The mono-, bis-, and trisadducts of C_{60} with tetraalkylcyclobutadiene groups were formed, and their electrochemical, photophysical, and thermal properties were compared. The thermal annealing process in device fabrication was revealed to be destructive for the new fullerene bis- and trisadducts, leading to large phase

separation and low PCEs. Epoxidation of cyclobutene confirmed that strong cofacial π-orbital interactions between C_{60} π-system and the double bond π-orbital contribute to raising the LUMO levels. Our results show that n-type materials for bulk heterojunction polymer solar cells can be chemically modified to fine-tune their electronic properties and thus the resulting open-circuit voltages in organic solar cells.

4. Experimental Section

Materials: C_{60} was purchased from SES Research, and aluminum chloride and alkynes were purchased from Sigma–Aldrich and used as received. Other materials including solvents and electrolyte salt were commercially available. Anhydrous solvents were obtained from a solvent purification system (Innovative Technologies).

Measurements: Reaction mixtures containing multiadducts of fullerenes were separated by 5PBB Cosmosil column (10 mm × 250 mm) from Nacalai Tesque, Inc. installed in Agilent Technologies ProsStar 210 High Pressure Liquid Chromatography (HPLC) system. ^{1}H and ^{13}C NMR spectra were taken on Varian Inova–500 spectrometers. Chemical shifts were reported in ppm and referenced to residual solvent peaks (CDCl₃: 7.26 ppm for ^{1}H, 77.20 ppm for ^{13}C). Thermally assisted direct analysis in real time (TA–DART)[48] high-resolution mass spectrometry (HRMS) was measured on LCQ DECA (Thermo–Finnigan LLC) with ID–CUBE source (IonSense, Inc.). Capillary temperature was 200 °C, and the capillary voltage was set to 15 V in positive-ion mode. Helium was used as the ionization gas. Bruker Daltonics Omniflex MALDI–TOF mass spectrometer was also used for mass determination. The matrix was prepared following a literature procedure,[49] containing 7,7,8,8-tetracyanoquinodimethane in THF (10 mg/mL) with 1% silver trifluoroacetate as a promoter. Molecules were dissolved in THF to 0.1 mg/mL concentration and the solution (2 µL) was mixed with matrix (20 µL). UV–vis absorption spectra were obtained using Agilent 8453 diode-array spectrophotometer. Electrochemical measurements were carried out in a glove box under nitrogen, using an Autolab PGSTAT 10 or PGSTAT 20 potentiostat (Eco Chemie) in a three-electrode cell configuration. A Pt button (1.6 mm in diameter) electrode, a Pt wire, and a quasi-internal Ag wire submerged in 0.01 M AgNO₃/0.1 M tetrabutylammonium hexafluorophosphate (TBAPF₆) in acetonitrile were used as a working electrode, a counter electrode, and a reference electrode, respectively, in 0.1 M TBAPF₆ toluene/acetonitrile (4:1) solution. The ferrocene/ferrocenium (Fc/Fc⁺) redox couple was used as an internal standard, with the half-wave potentials observed between 0.195–0.203 V vs Ag/Ag⁺ in toluene/acetonitrile (4:1) solution. Differential Scanning Calorimetry (DSC) was measured on a TA Instruments Q1000 DSC at scan rate of 10 °C/min over the range of 25 to 200 °C (or 35 to 200 °C). Thermogravimetric Analyses were performed with a TGA Q50 apparatus(TA Instruments) under nitrogen. Samples were heated at 10 °C/min from 30 °C to 800 °C. X-ray diffraction was measured using Cu Kα radiation on an Inel CPS 120 position-sensitive detector with a XRG 3000 generator using aluminum substrate during ca. 20 min collection time. Gaussian 03 software package was used for the structure optimization and the frequency calculation at the DFT level. B3LYP functional/6-31G (d,p) basis set was used for the computation.

Syntheses of TMCB-Mono and TMCB-Bis: In a flame dried 100 mL Schlenk flask, AlCl₃ (148 mg, 1.11 mmol) was dissolved in dry o-dichlorobenzene (o-DCB) (10 mL) and stirred at 0 °C under Ar. 2-Butyne (174 µL, 2.22 mmol) was added to the solution dropwise, and then o-DCB solution (20 mL) of C_{60} (400 mg, 0.555 mmol) was added. After 1 h of stirring to ensure formation of homogeneous phase, DMSO (0.2 mL, 2.33 mmol) was added dropwise and the solution was slowly warmed up to room temperature. Ethanol (50 mL) was poured, and the precipitate was filtered and washed with ethanol several times, and then dissolved in toluene/hexane (1:1, 100 mL). The solution was passed through silica gel pad (5 cm), and concentrated in vacuo. Monoadduct and Bisadduct

were separated by 5PBB Cosmosil column in toluene (4 mL/min) with yields of 31.9% (146.6 mg) and 16.5% (86.0 mg), respectively.

TMCB-Mono ^{1}H NMR (500 MHz, CDCl$_3$, δ): 2.07 (s, 6H), 1.97 (s, 6H). ^{13}C NMR (500 MHz, CDCl$_3$, δ): 154.62 (2C), 154.21 (2C), 147.24 (2C), 146.94 (2C), 146.91 (2C), 146.22 (2C), 146.14 (2C), 146.06 (2C), 145.53 (2C), 145.46 (2C), 145.39 (2C), 145.37 (2C), 145.35 (2C), 145.26 (2C), 144.69 (2C), 144.58 (2C), 143.21 (2C), 143.05 (2C), 142.86 (2C), 142.79 (2C), 142.49 (2C), 142.35 (2C), 142.31 (2C), 142.25 (2C), 142.11 (2C), 140.43 (2C), 140.37 (2C), 139.06 (2C), 137.75 (2C), 129.22 (1C), 128.41 (1C), 74.38 (2C), 60.38 (2C), 53.62 (CH$_2$Cl$_2$), 14.07 (2C), 11.56 (2C).

TMCB-Bis ^{1}H NMR (500 MHz, CDCl$_3$, δ): 2.22 (m, 3H), 2.05 (m, 3H), 2.03-2.02 (m, 3H), 1.98 (m, 3H), 1.89 (s, 3H), 1.85-1.84 (m, 3H), 1.75 (m, 3H), 1.66-1.64 (m, 3H). ^{13}C NMR (500 MHz, CDCl$_3$, δ): 157.49 (1C), 157.32 (1C), 155.46 (1C), 155.14 (1C), 155.10 (1C), 154.74 (1C), 154.62 (1C), 154.51 (1C), 154.44 (1C), 149.94 (1C), 149.91 (1C), 149.82 (1C), 149.60 (1C), 148.73 (1C), 148.71 (1C), 146.64 (1C), 148.26 (1C), 148.05 (1C), 147.91 (1C), 147.86 (1C), 147.75 (1C), 147.57 (1C), 147.28 (1C), 146.16 (1C), 145.97 (1C), 145.90 (1C), 145.77 (1C), 145.75 (1C), 145.59 (1C), 145.20 (1C), 145.08 (1C), 145.04 (2C), 144.76 (2C), 144.72 (1C), 144.59 (1C), 144.02 (1C), 143.72 (1C), 143.60 (1C), 142.66 (1C), 142.58 (1C), 142.55 (1C), 141.50 (1C), 141.43 (1C), 141.36 (1C), 141.24 (1C), 140.72 (1C), 139.99 (1C), 139.19 (1C), 138.62 (1C), 138.52 (1C), 138.06 (1C), 137.85 (1C), 137.16 (1C), 137.05 (1C), 129.22 (1C), 128.41 (2C), 125.49 (1C), 60.46 (2C), 60.10 (2C), 60.08 (2C), 60.01 (2C), 13.98 (2C), 13.87 (2C), 11.74 (1C), 11.49 (1C), 11.42 (1C), 11.24 (1C).

HRMS (ESI, m/z): Monoadduct [M+H]$^+$ calcd for C$_{68}$H$_{12}$, 829.1012; found, 829.04, Bisadduct [M]$^+$ calcd for C$_{76}$H$_{24}$, 937.0060; found, 936.99)

Synthesis of TMCB-Tris: In a flame dried 200 mL Schlenk flask, AlCl$_3$ (741 mg, 5.56 mmol) was dissolved in dry o-DCB (25 mL) and stirred at 0 °C under Ar. 2-Butyne (0.88 mL, 11.1 mmol) was added to the solution dropwise, and then o-DCB solution (50 mL) of C$_{60}$ (1.0 g, 1.39 mmol) was added. After 1 hour of stirring, DMSO (0.89 mL, 11.4 mmol) was added dropwise and the solution was slowly warmed up to room temperature. Ethanol (100 mL) was poured, and the precipitate was filtered and washed with ethanol several times, and then dissolved in toluene/hexane (1:1, 250 mL). The solution was passed through silica gel pad (5 cm), and concentrated in vacuo. 115 mg (7.9%) of the product was obtained after purification by 5PBB Cosmosil column in toluene (4 mL/min). ^{1}H NMR (500 MHz, CDCl$_3$, δ): 2.16-1.57 (m, 36H). ^{13}C NMR (500 MHz, CDCl$_3$, δ): 157.81 (2C), 157.68 (2C), 157.61 (2C), 155.49 (2C), 155.20 (2C), 155.09 (2C), 154.94 (2C), 154.57 (2C), 152.81 (2C), 151.51 (2C), 151.48 (2C), 151.13 (2C), 151.11 (2C), 149.70 (2C), 149.64 (2C), 149.57 (2C), 149.52 (2C), 149.45 (2C), 149.06 (2C), 148.94 (2C), 148.38 (2C), 148.37 (2C), 144.85 (2C), 144.84 (2C), 144.42 (2C), 144.26 (2C), 144.23 (2C), 115.33 (2C), 115.18 (2C), 114.84 (2C), 59.90 (6C), 59.29 (6C), 13.86 (2C), 13.77 (2C), 11.65 (2C), 11.41 (2C), 11.36 (2C), 11.28 (2C).

HRMS (MALDI–TOF, m/z): [M]$^+$ calcd for C$_{84}$H$_{36}$,1045.1871; found, 1045.22

Synthesis of TMCB-Ep: TMCB-Mono (102 mg, 0.123 mmol) was dissolved in chloroform (15 mL) in a 50 mL round-bottom flask in which a solution of 3-chloroperbenzoic acid (max. 77% purity, 76 mg, 0.339 mmol) in chloroform (5 mL) was added dropwise at 0 °C. The solution was slowly warmed up to room temperature during 7 h of stirring, and a major product spot was detected on a TLC plate. The reaction mixture was diluted with dichloromethane (75 mL), and extracted with NaOH aqueous solution several times. The organic layer was dried with MgSO$_4$ and concentrated in vacuo. 100 mg (96.1%) of the product was isolated after gradient silica column with 1:13 to 1:1 toluene/hexane eluent.

^{1}H NMR (500 MHz, CDCl$_3$, δ): 1.98 (s, 6H), 1.87 (s, 6H). ^{13}C NMR (500 MHz, CDCl$_3$, δ): 153.77 (2C), 153.69 (2C), 147.20 (2C), 146.76 (2C), 146.57 (2C), 146.30 (2C), 146.22 (2C), 146.21 (4C), 145.69 (2C), 145.55 (2C), 145.51 (2C), 145.43 (2C), 145.39 (2C), 144.75 (2C), 144.70 (2C), 143.35 (1C), 143.34 (1C), 142.94 (2C), 142.90 (2C), 142.55 (2C), 142.49 (2C), 142.26 (2C), 142.20 (2C), 142.19 (2C), 141.87 (2C), 140.64 (2C), 140.62 (2C), 138.87 (2C), 137.31 (2C), 71.38 (2C), 71.20 (2C), 62.46 (2C), 12.87 (2C), 12.12 (2C).

HRMS (ESI, m/z): [M+H]$^+$ calcd for C$_{68}$H$_{12}$O, 845.0961; found, 845.12

Syntheses of TBCB-Mono and TBCB-Bis. In a flame dried 50 mL Schlenk flask, AlCl$_3$ (150 mg, 1.12 mmol) was dissolved in dry o-DCB (15 mL) and stirred at 0 °C under Ar. 5-Decyne (0.41 mL, 2.28 mmol) was added to the solution dropwise, and then o-DCB solution (50 mL) of C$_{60}$ (200 mg, 0.28 mmol) was added. After 1 h of stirring, DMSO (0.2 mL, 2.33 mmol) was added dropwise and the solution was slowly warmed up to room temperature. Ethanol (35 mL) was poured, and the precipitate was filtered and washed with ethanol several times, and then dissolved in toluene/hexane (1:4, 150 mL). The solution was passed through silica gel pad (5 cm), and concentrated in vacuo. Monoadduct and bisadduct were separated by 5PBB Cosmosil column in toluene (4 mL/min) with yields of 40.1% (111.1 mg) and 24.1% (85.1 mg), respectively. 17.7% (35.5 mg) of C$_{60}$ was recovered.

TBCB-Mono ^{1}H NMR (500 MHz, CDCl$_3$/CS$_2$ 1:1, δ): 2.69-2.63 (m, 4H), 2.47-2.41 (m, 2H), 2.30-2.24 (m, 2H), 2.02-1.98 (m, 2H), 1.91-1.73 (m, 6H), 1.54-1.50 (m, 8H), 1.04-1.01 (t, 12H). ^{13}C NMR (500 MHz, CDCl$_3$/CS$_2$ 1:1, δ): 155.19 (2C), 153.81 (2C), 149.58 (2C), 147.25 (2C), 146.71 (2C), 146.23 (2C), 146.06 (2C), 145.99 (2C), 145.96 (2C), 146.87 (2C), 145.33 (2C), 145.18 (2C), 145.16 (4C), 144.53 (2C), 144.41 (2C), 143.08 (2C), 143.03 (1C), 142.89 (1C), 142.74 (2C), 142.71 (2C), 142.62 (2C), 142.31 (2C), 142.19 (2C), 142.09 (2C), 142.08 (2C), 141.95 (2C), 140.30 (2C), 140.09 (2C), 138.77 (2C), 137.78 (2C), 73.98(2C), 64.00 (2C), 31.46 (2C), 31.43 (2C), 29.51 (2C), 28.90 (2C), 24.34 (2C), 23.83 (2C), 14.31 (2C), 14.28 (2C).

TBCB-Bis ^{1}H NMR (500 MHz, CDCl$_3$/CS$_2$ 1:1, δ): 2.55-1.34 (m, 48H), 1.01-0.90 (m, 24H). ^{13}C NMR (500 MHz, CDCl$_3$/CS$_2$ 1:1, δ): 157.71 (2C), 157.67 (2C), 156.63 (2C), 155.55 (2C), 154.62 (2C), 154.05 (2C), 153.75 (2C), 153.56 (2C), 152.15 (2C), 149.50 (2C), 149.32 (2C), 148.98 (2C), 148.87 (2C), 148.47 (2C), 147.69 (2C), 147.11 (2C), 146.16 (2C), 145.00 (2C), 144.90 (2C), 144.85 (2C), 144.41 (2C), 144.27 (2C), 143.61 (2C), 142.57 (2C), 141.21 (2C), 141.14 (2C), 139.55 (2C), 138.83 (2C), 137.31 (2C), 136.81 (2C), 63.93 (2C), 63.87 (2C), 63.57 (2C), 63.55 (2C), 31.64 (1C), 31.54 (1C), 31.40 (1C), 31.37 (1C), 31.31 (1C), 31.26 (1C), 31.19 (1C), 31.12 (1C), 30.47 (1C), 30.03 (1C), 29.56 (1C), 29.38 (1C), 29.07 (1C), 28.92 (1C), 28.87 (1C), 28.72 (1C), 24.56 (1C), 24.38 (1C), 24.30 (1C), 24.04 (1C), 23.83 (1C), 23.81 (1C), 23.71 (1C), 23.65 (1C), 14.37 (2C), 14.32 (2C), 14.28 (2C), 14.19 (2C).

HRMS (ESI, m/z): [M+H]$^+$ calcd for C$_{80}$H$_{36}$, 997.2890; found, 997.23
HRMS (MALDI–TOF, m/z): [M]$^+$ calcd for C$_{100}$H$_{72}$, 1273.6448; found, 1273.62

Device Fabrication: Pre-patterned indium tin oxide (ITO)-coated glass substrates (Thin Film Devices, Inc.) were sonicated in acetone (30 min) and isopropanol (30 min) and oxygen plasma-cleaned (3 min) immediately prior to deposition of the PEDOT:PSS layer. PEDOT:PSS (2–5 wt% in water, Aldrich) was spin-coated in a nitrogen atmosphere at 4000 rpm and annealed at 150 °C (using a hotplate) for 15 min under nitrogen. A 40 nm PEDOT layer was thus obtained. Film thickness was determined by ellipsometry measurements on separate films prepared on silicon substrates. For the active layer, a 10 mg/mL solution of 1:1.2 P3HT:fullerene in 1,2-dichlorobenzene (DCB) was employed (in a representative example, P3HT (1.9 mg) and fullerene (2.3 mg) were dissolved in DCB (0.2 mL)). This solution (60 µL) was then spin-coated onto the PEDOT layer at 1000 rpm under nitrogen. The substrate was taken from the spin chuck and immediately placed under an inverted Petri dish inside the glovebox for 10 min to encourage solvent annealing from the small amount of residual DCB on the substrate. Next, the solar cells were placed on a 150 °C hotplate and annealed for 20 min under nitrogen. A 70 ± 5 nm active layer was thus obtained. Following this deposition procedure, the top electrode was deposited by thermal evaporation of a 25 nm thick film of Ca followed by 80 nm thick film of Al. The device area, as defined by the anode-cathode overlap, is 1.21 mm^2.

Device Characterization: Current density–voltage (J–V) measurements were recorded by a Keithley 6487 picoammeter both in the dark and under illumination. The devices were illuminated through the glass

www.MaterialsViews.com

ADVANCED
FUNCTIONAL
MATERIALS
www.afm-journal.de

FULL PAPER

substrate using an Oriel 91191 150 W full spectrum solar simulator. The illumination intensity was calibrated to 100 mW/cm^2 using an NREL-certified silicon photodiode. Spectral mismatch was not corrected for in these measurements.

FET Electron Mobility Measurement: Bottom-gate, bottom-contact FETs were made on Si substrates with a thermally-grown SiO$_2$ layer (500 nm) and 10 μm channel lengths (PCBM and TMCB-Mono). Top-gate, bottom-contact FETs were made on glass substrates with a PMMA layer (465 nm) top gate and 10 μm channel lengths (TMCB-bis and TMCB-tris).

Supporting Information

Supporting Information is available from Wiley Online Library or from the author.

Acknowledgements

[1] J. Roncali, *Acc. Chem. Res.* **2009**, *42*, 1719–1730.

[2] J. Chen, Y. Cao, *Acc. Chem. Res.* **2009**, *42*, 1709–1718.

[3] B. C. Thompson, J. M. J. Fréchet, *Angew. Chem. Int. Ed.* **2008**, *47*, 58–77.

[4] G. Yu, J. Gao, J. C. Hummelen, F. Wudl, A. J. Heeger, *Science* **1995**, *270*, 1789–1791.

[5] C. J. Brabec, M. Heeney, I. McCulloch, J. Nelson, *Chem. Soc. Rev.* **2011**, *40*, 1185–1199.

[6] D. Muhlbacher, M. Scharber, M. Morana, Z. G. Zhu, D. Waller, R. Gaudiana, C. J. Brabec, *Adv. Mater.* **2006**, *18*, 2884–2889.

[7] M. C. Scharber, D. Wuhlbacher, M. Koppe, P. Denk, C. Waldauf, A. J. Heeger, C. J. Brabec, *Adv. Mater.* **2006**, *18*, 789–794.

[8] F. G. Brunetti, X. Gong, M. Tong, A. J. Heeger, F. Wudl, *Angew. Chem. Int. Ed.* **2010**, *49*, 532–536.

[9] J. J. Dittmer, E. A. Marseglia, R. H. Friend, *Adv. Mater.* **2000**, *12*, 1270–1274.

[10] C. H. Woo, T. W. Holcombe, D. A. Unruh, A. Sellinger, J. M. J. Fréchet, *Chem. Mater.* **2010**, *22*, 1673–1679.

[11] J. L. Segura, N. Martin, D. M. Guldi, *Chem. Soc. Rev.* **2005**, *34*, 31–47.

[12] E. Champeil, C. Crean, C. Larraya, G. Pescitelli, G. Proni, L. Ghosez, *Tetrahedron* **2008**, *64*, 10319–10330.

[13] A. Penicaud, J. Hsu, C. A. Reed, A. Koch, K. C. Khemani, P. M. Allemand, F. Wudl, *J. Am. Chem. Soc.* **1991**, *113*, 6698–6700.

[14] M. D. Tzirakis, M. Orfanopoulos, *J. Am. Chem. Soc.* **2009**, *131*, 4063–4069.

[15] F. Diederich, C. Thilgen, *Science* **1996**, *271*, 317–323.

[16] M. A. Yurovskaya, I. V. Trushkov, *Russ. Chem. Bull.* **2002**, *51*, 367–443.

[17] J. C. Hummelen, B. W. Knight, F. Lepeq, F. Wudl, J. Yao, C. L. Wilkins, *J. Org. Chem.* **1995**, *60*, 532–538.

[18] D. W. Laird, R. Stegamat, H. Richter, Vejins, V. L. Scott, T. A. Lada, Patent WO/2008/018931 A2.

[19] A. Puplovskis, J. Kacens, O. Neilands, *Tetrahedron Lett.* **1997**, *38*, 285–288.

[20] C. J. Brabec, A. Cravino, D. Meissner, N. S. Sariciftci, T. Fromherz, M. T. Rispens, L. Sanchez, J. C. Hummelen, *Adv. Funct. Mater.* **2001**, *11*, 374–380.

[21] F. Huang, K.-S. Chen, H.-L. Yip, S. K. Hau, O. Acton, Y. Zhang, J. Luo, A. K. Y. Jen, *J. Am. Chem. Soc.* **2009**, *131*, 13886–13887.

[22] C. Piliego, T. W. Holcombe, J. D. Douglas, C. H. Woo, P. M. Beaujuge, J. M. J. Fréchet, *J. Am. Chem. Soc.* **2010**, *132*, 7595–7597.

[23] C. H. Woo, P. M. Beaujuge, T. W. Holcombe, O. P. Lee, J. M. J. Fréchet, *J. Am. Chem. Soc.* **2010**, *132*, 15547–15549.

[24] Y. Zhang, Y. Matsuo, C. Z. Li, H. Tanaka, E. Nakamura, *J. Am. Chem. Soc.* **2011**, *133*, 8086–8089.

[25] P. P. Khlyabich, B. Burkhart, B. C. Thompson, *J. Am. Chem. Soc.* **2011**, *133*, 1453 4–14537.

[26] F. B. Kooistra, J. Knol, F. Kastenberg, L. M. Popescu, W. J. H. Verhees, J. M. Kroon, J. C. Hummelen, *Org. Lett.* **2007**, *9*, 551–554.

[27] Y. J. He, H. Y. Chen, J. H. Hou, Y. F. Li, *J. Am. Chem. Soc.* **2010**, *132*, 137 7–1382.

[28] P. B. J. Driessen, H. Hogeveen, *J. Am. Chem. Soc.* **1978**, *100*, 1193–1200.

[29] S. Jankova, I. Cisarova, F. Uhlik, P. Stepnicka, M. Kotora, *Dalton Trans.* **2009**, 3137–3139.

[30] S. Jankova, M. Dracinsky, I. Cisarova, M. Kotora *Eur. J. Org. Chem.* **2008**, 4 7–51.

[31] F. Wudl, *Acc. Chem. Res.* **1992**, *25*, 157–161.

[32] Y. He, G. Zhao, B. Peng, Y. Li, *Adv. Funct. Mater.* **2010**, *20*, 3383–3389.

[33] C. Liu, S. Xiao, X. Shu, Y. Li, L. Xu, T. Liu, Y. Yu, L. Zhang, H. Liu, Y. Li, *ACS Appl. Mater. Interfaces* **2012**, *4*, 1065–1071.

[34] D. M. Guldi, *J. Phys. Chem. B* **2000**, *104*, 1483–1489.

[35] M. M. Wienk, J. M. Kroon, W. J. H. Verhees, J. Knol, J. C. Hummelen, P. A. van Hal, R. A. J. Janssen, *Angew. Chem., Int. Ed.* **2003**, *42*, 3371–3375.

[36] K. M. Kadish, X. Gao, E. V. Caemelbecke, T. Suenobu, S. Fukuzumi, *J. Phys. Chem. A* **2000**, *104*, 3878–3883.

[37] Y. Murata, K. Komatsu, T. S. M. Wan, *Tetrahedron Lett.* **1996**, *37*, 7061–7064.

[38] Z.-X. Chen, G.-W. Wang, *J. Org. Chem.* **2005**, *70*, 2380–2383.

[39] Y. Tajima, T. Hara, T. Honma, S. Matsumoto, K. Takeuchi. *Org. Lett.* **2006**, *8*, 3203–3205.

[40] J. Milliken, T. M. Keller, A. P. Baronavski, S. W. Mcelvany, J. H. Callahan, H. H. Nelson, *Chem. Mater.* **1991**, *3*, 386–387.

[41] J. L. Delgado, F. Oswald, F. Cardinali, F. Langa, N. Martin, *J. Org. Chem.* **2008**, *73*, 3184–3188.

[42] N. Martin, M. Altable, S. Filippone, A. Martin-Domenech, L. Echegoyen, C. M. Cardona, *Angew. Chem., Int. Ed.* **2006**, *45*, 110–114.

[43] S. Osuna, K. N. Houk, *Chem. Eur. J.* **2009**, *15*, 13219–13231.

[44] S. Osuna, J. Morera, M. Cases, K. Morokuma, M. Sola, *J. Phys. Chem. A* **2009**, *113*, 9721–9726.

[45] M. Solá, J. Mestres, J. Martí, M. Duran, *Chem. Phys. Lett.* **1994**, *231*, 325–330.

[46] A. Maurano, R. Hamilton, C. G. Shuttle, A. M. Ballantyne, J. Nelson, B. O'Regan, W. Zhang, I. McCulloch, H. Azimi, M. Morana, C. J. Brabec, J. R. Durrant, *Adv. Mater.* **2010**, *22*, 4987–4992.

[47] C. A. Hunter, J. K. M. Sanders, *J. Am. Chem. Soc.* **1990**, *112*, 5525–5534.

[48] J. Krechmer, J. Tice, E. Crawford, B. Musselman, *Rapid Commun. Mass Spectrom.* **2011**, *25*, 2384–2388.

[49] R. Jasti, J. Bhattacharjee, J. B. Neaton, C. R. Bertozzi, *J. Am. Chem. Soc.* **2008**, *130*, 17646–17647.